An Observed Connection between the North Atlantic Oscillation and the Madden–Julian Oscillation

HAI LIN AND GILBERT BRUNET

MRD/ASTD, Environment Canada, Dorval, Québec, Canada

JACQUES DEROME

Department of Atmospheric and Oceanic Sciences, McGill University, Montréal, Québec, Canada

(Manuscript received 6 March 2008, in final form 9 July 2008)

ABSTRACT

Based on the bivariate Madden–Julian oscillation (MJO) index defined by Wheeler and Hendon and 25 yr (1979–2004) of pentad data, the association between the North Atlantic Oscillation (NAO) and the MJO on the intraseasonal time scale during the Northern Hemisphere winter season is analyzed. Time-lagged composites and probability analysis of the NAO index for different phases of the MJO reveal a statistically significant two-way connection between the NAO and the tropical convection of the MJO. A significant increase of the NAO amplitude happens about 5–15 days after the MJO-related convection anomaly reaches the tropical Indian Ocean and western Pacific region. The development of the NAO is associated with a Rossby wave train in the upstream Pacific and North American region. In the Atlantic and African sector, there is an extratropical influence on the tropical intraseasonal variability. Certain phases of the MJO are preceded by the occurrence of strong NAOs. A significant change of upper zonal wind in the tropical Atlantic is caused by a modulated transient westerly momentum flux convergence associated with the NAO.

1. Introduction

The North Atlantic Oscillation (NAO) is a dominant mode of atmospheric variability in the Northern Hemisphere (e.g., Wallace and Gutzler 1981; Barnston and Livezey 1987). The main characteristics of the NAO include a dipole spatial structure in sea level pressure over the North Atlantic, with one center over Greenland and the other center of opposite sign along the North Atlantic between 35° and 40°N, and an equivalent barotropic vertical structure. With a time scale ranging from days to decades, the NAO has long been recognized as a major circulation pattern influencing the weather from eastern North America to Europe (e.g., van Loon and Rogers 1978; Hurrell 1995).

It has been suggested that the primary mechanism for the NAO is the internal dynamics of the extratropical circulation. The variability of the Northern Hemisphere annular mode, or the Arctic Oscillation (AO), which is well correlated with the NAO (Thompson and Wallace 1998), is associated with wave–mean flow interactions (e.g., Limpasuvan and Hartmann 1999). Franzke et al. (2004) pointed out that the NAO may be a result of midlatitude wave breaking. The mechanism related to extratropical atmospheric internal dynamics implies a lack of predictability for the NAO variability at an extended range.

Searches for sources of the NAO variability that are external to the extratropical atmosphere are of practical as well as scientific importance. Candidates include the forcing from the underlying sea surface temperature (SST) anomaly in the extratropical North Atlantic (e.g., Palmer and Sun 1985; Peng and Whitaker 1999), coupling with the stratosphere (e.g., Baldwin et al. 2003), and interaction with the snow cover in Eurasia (e.g., Cohen et al. 2001). A link between the NAO and the diabatic heating in the tropics has been suggested by several recent studies. On an interannual time scale, a positive phase of the NAO is observed to be associated with a reduction of diabatic heating in the tropical western and central Pacific (e.g., Pozo-Vázquez et al. 2001; Lin et al. 2005; Li et al. 2006). On a decadal and

Corresponding author address: Dr. Hai Lin, MRD/ASTD, Environment Canada, 2121 route Trans-Canadienne, Dorval, QC H9P 1J3, Canada.
E-mail: hai.lin@ec.gc.ca

DOI: 10.1175/2008JCLI2515.1

longer time scale, a gradual change of the SST in the equatorial Indian Ocean is likely to be linked to a slow variation of the NAO (e.g., Hoerling et al. 2001; Greatbatch et al. 2003). Because of the small signal-to-noise ratio and the model dependence of the atmospheric response, whether and how the NAO is related to a forcing external to the extratropical atmosphere are far from clearly established.

The Madden–Julian oscillation (MJO) is the dominant mode of intraseasonal variability in the tropics, which is characterized by a large-scale zonal-vertical cell propagating eastward along the equator with a period of 30–60 days (e.g., Madden and Julian 1971, 1994). The maximum convective activity associated with the MJO occurs over the warm waters of the Indian Ocean and western Pacific where the signal moves eastward at a relatively slow speed ($\sim$5 m s^{-1}), whereas in the Western Hemisphere the MJO is less well coupled with convection and propagates faster ($\sim$15 m s^{-1}; e.g., Zhang 2005). The mechanism for the generation of the MJO is not well understood, although there have been suggestions that processes within the tropical atmosphere such as latent heat release, evaporation, and radiation are important (e.g., Lau and Peng 1987; Emanuel 1987; Wang 1988; Hu and Randall 1994).

Through the variability of tropical diabatic heating, the MJO influences the extratropical circulations by driving teleconnection patterns (e.g., Lau and Phillips 1986; Knutson and Weickmann 1987, Ferranti et al. 1990; Higgins and Mo 1997; Matthews et al. 2004). Among the various studies, there is a general agreement regarding the extratropical anomaly in the North Pacific sector associated with the MJO convection; that is, a cyclonic (anticyclonic) anomaly in the North Pacific near 45°N, 180° is likely to be linked to the tropical enhanced (suppressed) convection of the MJO when it moves eastward toward the date line. In the other extratropical regions, however, the results are less consistent, presumably because of different analysis techniques and relatively short periods of datasets used. The influence of extratropical atmospheric flows on the tropical low-frequency variability has also been observed (e.g., Liebmann and Hartmann 1984; Hsu et al. 1990; Hsu 1996).

An important component in the coherent fluctuations between the tropical intraseasonal variability and the extratropical circulation is the possible link between the NAO and the MJO. Understanding such a link is crucial for answering questions related to the origin of both the NAO and MJO and atmospheric predictability on an intraseasonal time scale. Zhou and Miller (2005) investigated the relationship between the AO and the MJO in the Northern Hemisphere winter season, and found that a high (low) AO phase tends to be coupled with a strong (suppressed) convective activity associated with the MJO over the Indian Ocean. They argued that the MJO influences the AO polarity by altering the geopotential height anomaly in the North Pacific sector through meridional dispersion of Rossby waves. This result is supported by L'Heureux and Higgins (2008), who analyzed the boreal winter links between the MJO and the AO using observational data and model output.

Although highly correlated, whether the AO and NAO are the same phenomenon is not without a debate (Deser 2000; Ambaum et al. 2001; Wallace and Thompson 2002). The NAO is considered to be a more localized circulation pattern in the North Atlantic sector. Without the contribution of the North Pacific center of the AO, how the NAO is connected with the MJO is of great interest. Another important question to ask is what is the role played by the NAO in the NAO–MJO connection. With a primitive equation dry atmospheric model [simplified general circulation model (SGCM)] with time-independent forcing, Lin et al. (2007a, hereafter LBD07) were able to simulate tropical intraseasonal variability that had many features similar to the MJO. They argued that interactions between the tropical and extratropical flows are responsible for the simulated intraseasonal variability. A tropical influence on the extratropical flow occurred in the North Pacific region with a northward wave activity flux, while in the North Atlantic sector a strong extratropical influence on the tropics was evidenced by a southward wave activity flux that forced an equatorial Kelvin wave propagating eastward. An objective of the present study is to see whether this two-way interaction can be observed in the real atmosphere.

In this study, we look at the interaction between the NAO and the MJO on an intraseasonal time scale. Section 2 describes the data and methodology of analysis. In section 3, lagged composites of the NAO index with respect to the MJO phases are presented. Section 4 discusses the time evolution the extratropical flow anomaly associated with two phases of the MJO and the wave activity flux. In section 5, the influence of the NAO on the tropical intraseasonal variability is analyzed. Section 6 gives a summary and discussion.

2. Data and methodology

The daily data of the National Centers for Environmental Prediction–National Center for Atmospheric Research (NCEP–NCAR) global reanalysis of atmospheric fields (Kalnay et al. 1996) are used in this study. Variables used here include geopotential height on 500 hPa, zonal and meridional winds on 200 and 850 hPa.

To represent the MJO, the Real-Time Multivariate MJO (RMM) index of Wheeler and Hendon (2004) is

used. The daily values of RMM1 and RMM2 is obtained from the Australian Bureau of Meteorology Web site (http://www.bom.gov.au/bmrc/clfor/cfstaff/matw/maproom/RMM/). The RMM1 and RMM2 were calculated by projecting the combined fields of 15°S–15°N meridionally averaged satellite-observed outgoing longwave radiation (OLR) and zonal winds at 850 and 200 hPa onto the two leading empirical orthogonal function (EOF) structures as derived using the same meridionally averaged variables. The time series of RMM1 and RMM2 vary mostly on the intraseasonal time scale, and the associated three-dimensional flow structure captures the MJO variability.

To represent the tropical convection associated with the MJO, the pentad data of the Climate Prediction Center (CPC) Merged Analysis of Precipitation (CMAP; Xie and Arkin 1997) are used. Additional data applied to represent a proxy for tropical convection are the daily averaged OLR data from the National Oceanic and Atmospheric Administration (NOAA) polar-orbiting series of satellites (Liebmann and Smith 1996).

The horizontal resolution for the NCEP–NCAR reanalysis, the OLR, and the CMAP precipitation is 2.5° × 2.5°. The daily values of the NCEP–NCAR reanalysis, the OLR, and the MJO index are averaged for consecutive five days to construct pentad data. The analysis is conducted for 25 extended winters from 1979/80 to 2003/04, where the extended winter is defined to be the 36 pentads starting from the pentad of 2–6 November and ending at the pentad of 26–30 April, resulting in a total of 900 pentads. To match the pentad definition of the CMAP precipitation, the 24th pentad of each extended winter always covers a period from 25 February to 1 March, no matter if it is a leap year or not. Thus in the case of a leap year, the data for that ''pentad'' are actually an average for six days.

The seasonal cycle, which is the annual mean and first two harmonics of the 25-yr pentad climatology, is first removed for each grid point. The mean for each extended winter is then removed in order to eliminate interannual variability. The seasonal cycle and interannual variability have already been removed in the RMM1 and RMM2 data.

To identify the NAO pattern, a rotational EOF analysis technique (REOF) is used, following Barnston and Livezey (1987). The REOF is conducted for the monthly mean 500-hPa geopotential height over the Northern Hemisphere using the NCEP–NCAR reanalyses from 1948 to 2004. Monthly mean anomalies for all 12 calendar months are used. The NAO is defined as the second REOF mode, with its spatial distribution shown in Fig. 1. The structure is largely localized in the Atlantic sector, and almost no height anomaly can be seen in the North Pacific, a clear contrast to the AO structure (e.g., Thompson and Wallace 1998). Since the NAO variability has the largest variance in the cold season, the pattern is thus dominated by characteristics in winter. Similar definition of the NAO was used in Johansson (2007). To test the sensitivity of the result to the definition of the NAO, all the calculations presented below have been repeated with two other definitions, that is, REOF of winter months only and of winter seasonal mean (December, January, and February) 500-hPa geopotential height, and no change to the conclusion was found. The NAO index is calculated as the projection of the pentad 500-hPa geopotential height anomaly onto this pattern and normalized so that its standard deviation over the 900 winter pentads is unity.

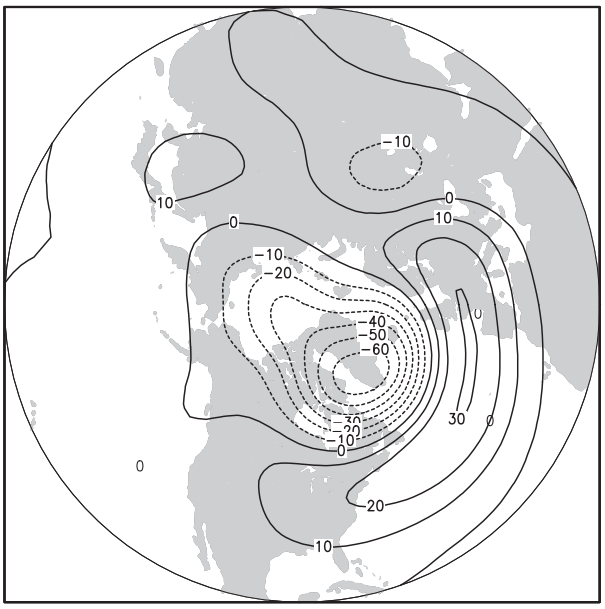

FIG. 1. The NAO pattern used in this study, which is the second mode of a rotated EOF analysis of monthly mean 500-hPa geopotential height, represented as regressions of monthly mean 500-hPa height onto the time expansion coefficient. The magnitude corresponds to one std dev of the time coefficient. The contour interval is 10 m. Contours with negative values are dashed.

3. Composites of the NAO index with respect to MJO phases

a. Tropical precipitation

Following Wheeler and Hendon (2004), an MJO state can be represented as a point in the two-dimensional phase space of RMM1 and RMM2. The distance of a point from the origin $\sqrt{\mathrm{RMM1}^2 + \mathrm{RMM2}^2}$ can be considered the MJO amplitude, and an eastward propagation of the MJO is reflected by a counterclockwise

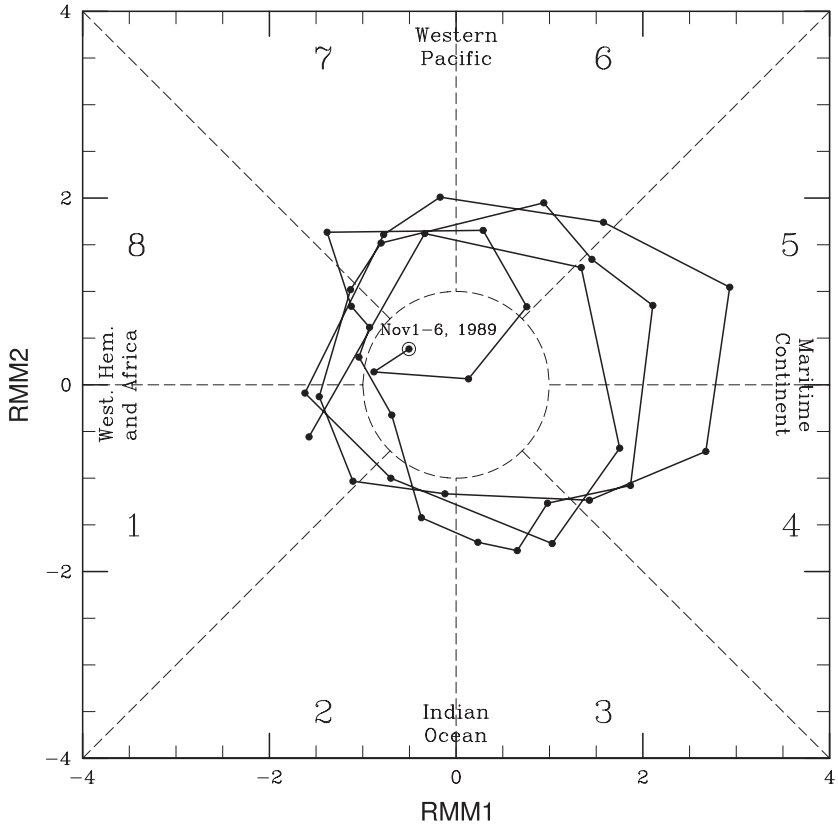

FIG. 2. Trajectory of the observed pentad MJO index in the RMM1–RMM2 phase space for all the pentads in the extended winter of 1989/90.

movement in the phase space plot. As an example, shown in Fig. 2 are the MJO states for all the pentads in the extended winter of 1989/90. Apart from the weak MJO area, where the MJO has an amplitude less than 1, eight phases are defined in Fig. 2. Indicated for each quadrant of the plot is the location of the enhanced convection associated with the MJO.

Starting from the RMM1 and RMM2 pentad values for the extended winter season from 1979 to 2004, the pentads that belong to each of the eight phases of the MJO are identified. Listed in Table 1 are the number of pentads and the averaged MJO amplitude for each phase. It can be seen that phases 2–4 and 6–7 have a relative high frequency of appearance. The maximum amplitude of the MJO tends to occur in phases 3–4, which correspond to an enhanced convection over the warm water between the Indian Ocean and the Maritime Continent, consistent with previous studies.

The simultaneous composites of the CMAP precipitation anomaly in the tropics for different MJO phases are shown in Fig. 3. The distributions of precipitation anomalies agree well with the winter composites of the OLR for the MJO phases as presented in Wheeler and Hendon (2004, their Fig. 8). Starting from phase 1, enhanced convection and precipitation develop over Africa and the western Indian Ocean. In the subsequent phases, the positive precipitation anomaly moves eastward along the equator, and gets dissipated in phase 1 over the central Pacific after a whole cycle of the MJO. The maximum precipitation anomaly occurs in phase 3–4 when it is located between the Indian Ocean and the Maritime Continent. When the positive precipitation anomaly reaches the western Pacific in phase 5, a negative anomaly starts to build over Africa and the western Indian Ocean, which repeats the process of its positive counterpart. The enhanced (reduced) convection and precipitation reaches the tropical central Pacific in phases 6–8 (phases 2–4).

TABLE 1. Number of pentads and averaged amplitude for each phase of the MJO.

Phase	1	2	3	4	5	6	7	8
No. of pentads	55	79	78	78	63	71	87	66
Mean amplitude	1.67	1.66	1.81	1.78	1.66	1.70	1.62	1.75

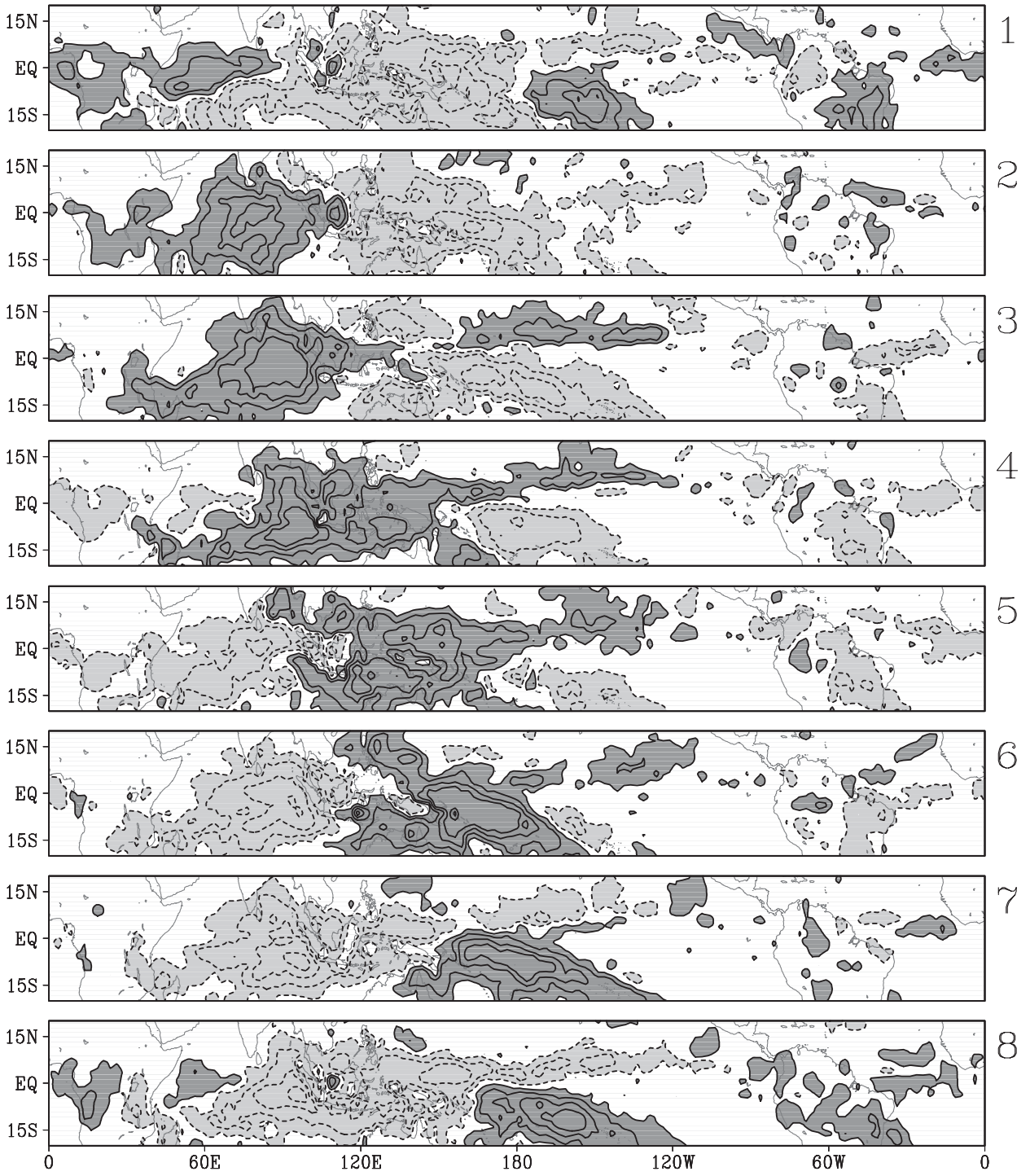

FIG. 3. Simultaneous composites of the CMAP precipitation anomaly in the tropics for different MJO phases. The contour levels for positive values are 0.5, 1.5, 3.0, and 4.5 mm day^{-1} and are in solid, while those for negative values are −0.5, −1.5, −3.0, and −4.5 mm day^{-1} and are in dashed. Shaded in dark gray are areas with precipitation rate anomaly greater than 0.5 mm day^{-1}, whereas in light gray are those with precipitation rate anomaly smaller than −0.5 mm day^{-1}. The phase numbers are marked on the right of each panel.

TABLE 2. Lagged composites of the NAO index with respect to each MJO phase. Lag *n* means that the NAO lags the MJO of the specific phase by *n* pentads, while lag –*n* represents that the NAO leads the MJO by *n* pentads. Numbers in bold represent those that pass a 0.05 significance level.

Phase	1	2	3	4	5	6	7	8
Lag −5	0.05	−0.11	**−0.39**	0.21	0.00	0.21	**0.28**	0.14
Lag −4	−0.01	**−0.26**	80.18	0.18	0.17	**0.28**	0.10	0.11
Lag −3	0.00	**−0.29**	0.14	0.15	0.21	0.12	0.12	−0.08
Lag −2	−0.09	0.02	0.22	0.02	0.08	**0.26**	0.00	−0.20
Lag −1	−0.23	0.10	0.09	0.07	0.06	0.14	−0.17	−0.17
Lag 0	−0.16	0.20	0.07	0.20	0.06	−0.02	−0.03	**−0.41**
Lag 1	−0.18	**0.26**	**0.27**	**0.26**	0.02	0.00	**−0.25**	**−0.35**
Lag 2	0.14	**0.34**	**0.36**	0.19	−0.06	**−0.31**	**−0.33**	**−0.29**
Lag 3	0.10	**0.35**	0.13	0.10	−0.08	**−0.35**	**−0.41**	−0.12
Lag 4	0.04	0.17	0.10	0.01	−0.24	**−0.35**	**−0.31**	−0.02
Lag 5	0.10	0.19	−0.01	**−0.27**	−0.11	−0.20	−0.16	0.07

TABLE 3. Lagged percentage probability of the NAO index with respect to each MJO phase and lag. Lag *n* means that the NAO lags the MJO of the specific phase by *n* pentads, while lag –*n* represents that the NAO leads the MJO by *n* pentads. Positive values are for upper tercil, while negative are for low tercil. Values shown are only for those pass a 0.05 significance level according to a Monte Carlo test. Values greater than 45 are significant at the 0.01 level.

Phase	1	2	3	4	5	6	7	8
Lag −5		−35	−40			+49	+49	
Lag −4						+52	+46	
Lag −3		−40					+46	
Lag −2						+50		
Lag −1								
Lag 0				+45				−42
Lag 1			+47	+45				−46
Lag 2		+47	+50	+42		−41	−41	−42
Lag 3		+48				−41	−48	
Lag 4						−39	−48	
Lag 3				−41				

b. Composites of the NAO index

To analyze the connection between the NAO and the MJO, lagged composites are calculated for the NAO index for different phases of the MJO, which are presented in Table 2. Lag *n* means that the NAO lags the MJO of the specific phase by *n* pentads, while lag $-n$ represents that the NAO leads the MJO by *n* pentads. Numbers in bold represent those that are different from zero at a 0.05 significance level according to a Student's *t* test. A two-way interaction between the NAO and the MJO is evident. A negative NAO leads phases 2 and 3 of the MJO by 3∼5 pentads, whereas a positive NAO precedes phases 6 and 7 by 2∼5 pentads. On the other hand, when the MJO leads the NAO, significant positive NAOs are found for phases 2–4, and negative NAOs for phases 6–8, indicating a significant influence of the tropical MJO on the extratropical NAO variability. On average, the NAO index is positive (negative) 5–15 days after the MJO is detected in phases 2–4 (phases 6–8). The magnitude of the composite NAO index that is statistically significant at a 0.05 level ranges from 0.25∼0.41, implying that the amplitude of the NAO associated with the MJO variability is about 25%∼41% of its standard deviation in the extended winter season.

c. Probability of the NAO index in the upper and lower terciles

Here we present another measure for the connection between the NAO and the MJO. The NAO index for all the pentads are categorized as below normal, near normal, and above normal. Pentads with an above-normal NAO are those with an NAO index greater than 0.43 (as the NAO index is normalized by its standard deviation), whereas pentads with a below-normal NAO are those with an index smaller than −0.43, and the rest are categorized as near normal. Each of the three categories has a probability of 33%.

We investigate the probability of an above- (below-) normal NAO index when the MJO is in a given phase, also referred to as the probability of an upper (lower) tercile. The probability of upper (lower) tercile for a given MJO phase and a given lag is obtained by counting the number of pentads for which the NAO index is above (below) normal and then dividing by the total number of pentads in that composite. Statistical significance for the probability composite is assessed using a Monte Carlo approach, where we randomly shuffle the order of years for the NAO index and recompute the composite probability. This is repeated 500 times. We then count how many times the probability exceeds that of the actual composite. If fewer than 5% of the 500 simulations have a probability greater than that of the actual composite, we say that the probability composite passes a 0.05 significance level.

Listed in Table 3 are the NAO probabilities for the eight MJO phases with lags from −5 to 5 pentads. Positive values are for the upper tercile and negative for the lower tercile. Listed are only those that pass a 0.05 significant level according to the Monte Carlo test.

In general, the probability results are consistent with the composites of the NAO index itself of Table 2. When the NAO leads the MJO, there is a high probability that a negative NAO leads phases 2 and 3 by 3∼5 pentads, whereas a positive NAO leads phases 6 and 7 by 2∼5 pentads. On the other hand, a systematic connection between the NAO and MJO is found when the MJO leads the NAO. Significant large probabilities of the

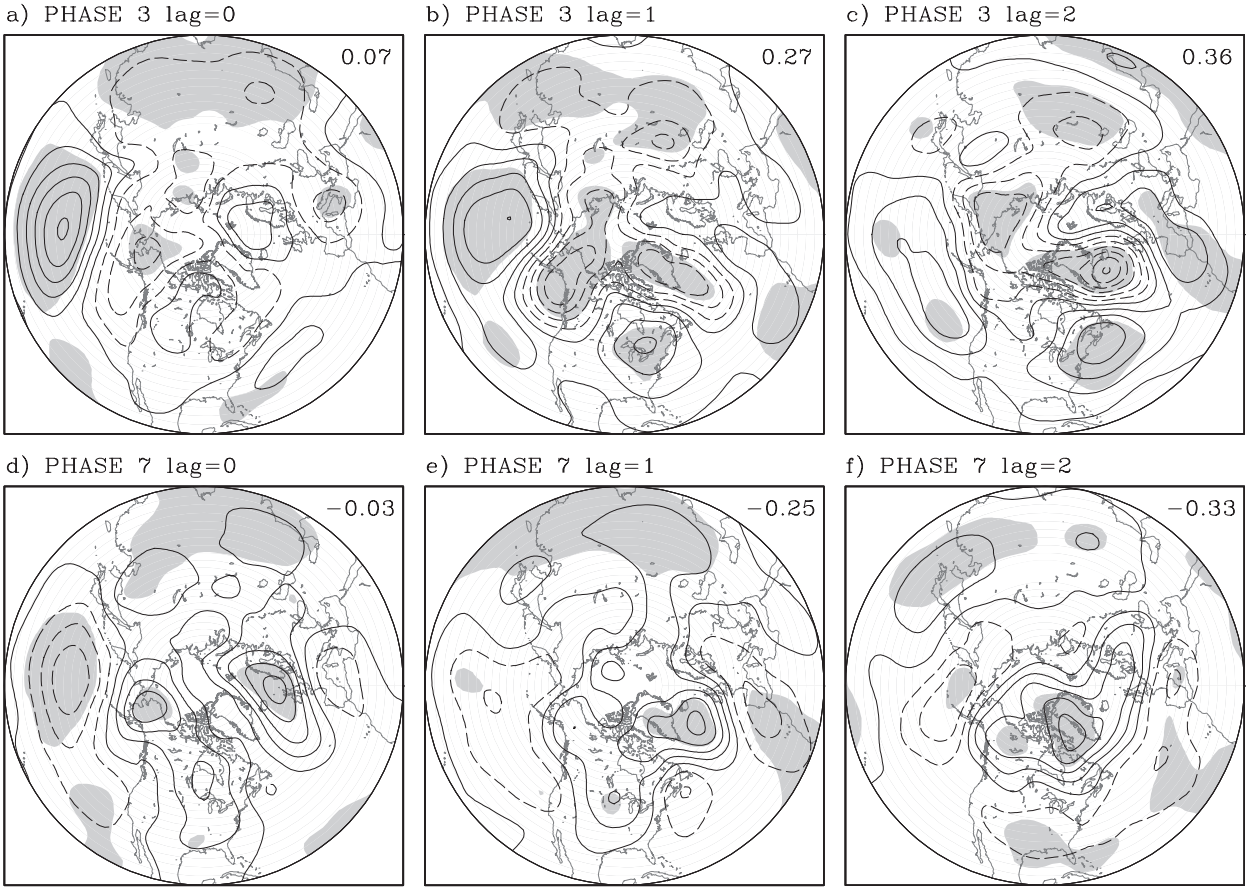

FIG. 4. Lagged composites of 500-hPa geopotential height anomaly for MJO (a)–(c) phase 3 and (d)–(f) phase 7. Contour interval is 10 m. Contours with negative values are dashed. Shaded areas represent those where the composite anomaly is different from zero at a 0.05 significance level according to a Student's *t* test. The numbers in the upper right corners are the projection of the composite anomalies onto the NAO pattern of Fig. 1 (same as values shown in Table 2).

NAO index in the upper tercile are observed for phases 2–4 and large probabilities in the lower tercile for phases 6–8. Hence, a positive (negative) NAO is likely to happen 5–15 days after the MJO is detected in phases 2–4 (phases 6–8), which correspond to an enhanced (reduced) precipitation over the Indian Ocean and Maritime Continent and a reduced (enhanced) convective activity near the tropical central Pacific (Fig. 3).

4. Evolution of extratropical circulation anomaly

In this section, we take a look at the evolution of the extratropical circulation anomaly associated with the MJO and its link to the NAO pattern. As shown in Table 2, the NAO is significantly influenced by the tropical convection when the MJO is in one of the two phase groups, that is, phases 2–4 and phases 6–8. Here we analyze in detail the lagged composites of the extratropical circulation anomaly and see how it evolves after the MJO is observed in these two phase groups. For simplicity, we use phase 3 and phase 7 to represent the two phase groups, respectively.

a. 500-hPa geopotential height

Shown in Fig. 4 are the lagged composite maps of 500-hPa geopotential height anomaly for MJO phase 3 (Figs. 4a–c) and phase 7 (Figs. 4d–f). Lag *n* indicates that the 500-hPa height anomaly lags the MJO of the specific phase by *n* pentads. Shaded areas represent those where the composite anomaly is different from zero at a 0.05 significance level according to a Student's *t* test.

For MJO phase 3, on the simultaneous composite map (Fig. 4a), a dominant feature is that a significant positive height anomaly is formed over the North Pacific centered at 45°N, 180°, associated with a depressed convection and precipitation over the equatorial central Pacific (phase 3 in Fig. 3), a robust feature consistent with previous studies (e.g., Matthews et al. 2004). Together with the downstream negative anomaly over

Alaska and the positive anomaly over Canada, that are less statistically significant, these circulation anomalies form a wave train reminiscent of a negative phase of the Pacific–North American (PNA) pattern except for a westward phase shift. This tropical–extratropical connection is also reminiscent of a La Niña event when there is an anomalous tropical cooling near the date line associated with a below-normal SST in the tropical Pacific (e.g., Hoerling et al. 1997).

One pentad later (Fig. 4b), the wave pattern shows downstream dispersion, with significant height anomaly centers developing downstream and the North Pacific center weakening. At the same time, a negative height anomaly deepens rapidly over the Greenland region. After another pentad (Fig. 4c), significant development of circulation anomalies takes place in the North Atlantic sector, forming a pattern that projects strongly to a positive NAO.

For MJO phase 7, the simultaneous composite map (Fig. 4d) shows a similar feature as that of phase 3 except for a reversal of sign. Associated with an enhanced convection and precipitation over the equatorial central Pacific (phase 7 in Fig. 3), a significant negative height anomaly is seen over the North Pacific. This is reminiscent of an El Niño event and a positive phase of the PNA. In the following pentads (Figs. 4e,f), the North Pacific negative height anomaly weakens, and a pattern develops in the North Atlantic sector that projects to a negative NAO.

For both MJO phases 3 and 7, a full development of circulation anomalies in the extratropical Atlantic happens two pentads after the tropical thermal forcing anomaly is moved to the date line longitude. The timing of this development is consistent with previous studies, that have shown that the extratropical response to a tropical thermal forcing develops in about two weeks (e.g., Jin and Hoskins 1995; Matthews et al. 2004; Lin et al. 2007b).

b. *Wave activity flux*

To analyze the time evolution of the wave activity flux associated with the extratropical circulation anomalies, the wave activity flux vector (**W** vector) proposed by Takaya and Nakamura (2001) is calculated, which is based on the conservation of wave activity pseudomomentum. This formulation of wave activity flux vector allows snapshots of wave dispersion to be taken in each stage of the evolution of the circulation anomalies. The horizontal components of the **W** vector can be given by

$$\mathbf{W} = \frac{1}{2|\mathbf{U}|}\begin{bmatrix} U(\psi_x^2 - \psi\psi_{xx}) + V(\psi_x\psi_y - \psi\psi_{xy}) \\ U(\psi_x\psi_y - \psi\psi_{xy}) + V(\psi_y^2 - \psi\psi_{yy}) \end{bmatrix}, \quad (1)$$

where ψ is the perturbation streamfunction and the subscripts represent partial derivatives. Here $\mathbf{U} = (U, V)$ is the 200-hPa two-dimensional time mean zonal and meridional winds for extended winter. The wave activity flux vectors are calculated based on lagged composite maps of the 200-hPa streamfunction with respect to the MJO phases.

Figure 5 depicts the wave activity flux with respect to MJO phase 3 for lags 0, 1, and 2 pentads. For clarity and simplicity, the maps are shown for the extratropical North Pacific, North American, and North Atlantic sectors. Also shown on the maps as contours is the 200-hPa streamfunction anomaly composite. The 200-hPa streamfunction anomaly distributions are consistent with those of the 500-hPa geopotential height (Figs. 4a–c). Such an equivalent barotropic vertical structure is not surprising for extratropical circulation anomalies as remote responses to a tropical forcing. On the simultaneous composite map (Fig. 5a), a strong wave activity flux is clearly seen originating from the subtropical Pacific and pointing northeastward, along the path of the wave train. With further northeastward penetration of the wave activity flux (Fig. 5b), downstream circulation anomaly centers get enhanced. By lag 2, the North Pacific anomaly centers become dissipated and the anomaly pattern in North Atlantic becomes very strong, associated with northeastward wave activity flux in the west and southeastward flux in the east. The wave activity flux associated with the MJO convection agrees well with that simulated by the SGCM in LBD07, indicating that a similar dynamical process is in action in both the observation and the model. As discussed in LBD07, the strong southward wave activity flux in the subtropical Atlantic may lead to further development of tropical intraseasonal variability.

Wave activity flux with respect to MJO phase 7 (not shown) shows a similar downstream propagation, although the wave activity flux from the Pacific is weaker than that in MJO phase 3. As the wave activity is a squared quantity, its flux is independent of the sign of the wave patterns. The sign of the anomaly centers is determined by the Rossby wave source in the subtropical Pacific associated with upper divergence or convergence of the tropical heating source (e.g., Sardeshmukh and Hoskins 1988).

5. Influence of the NAO on the tropical intraseasonal variability

As is discussed in the last section, a possible extratropical influence on the tropics is in the North Atlantic sector, where a strong southward wave activity flux into the tropics is found. In LBD07, a set of linear experiments

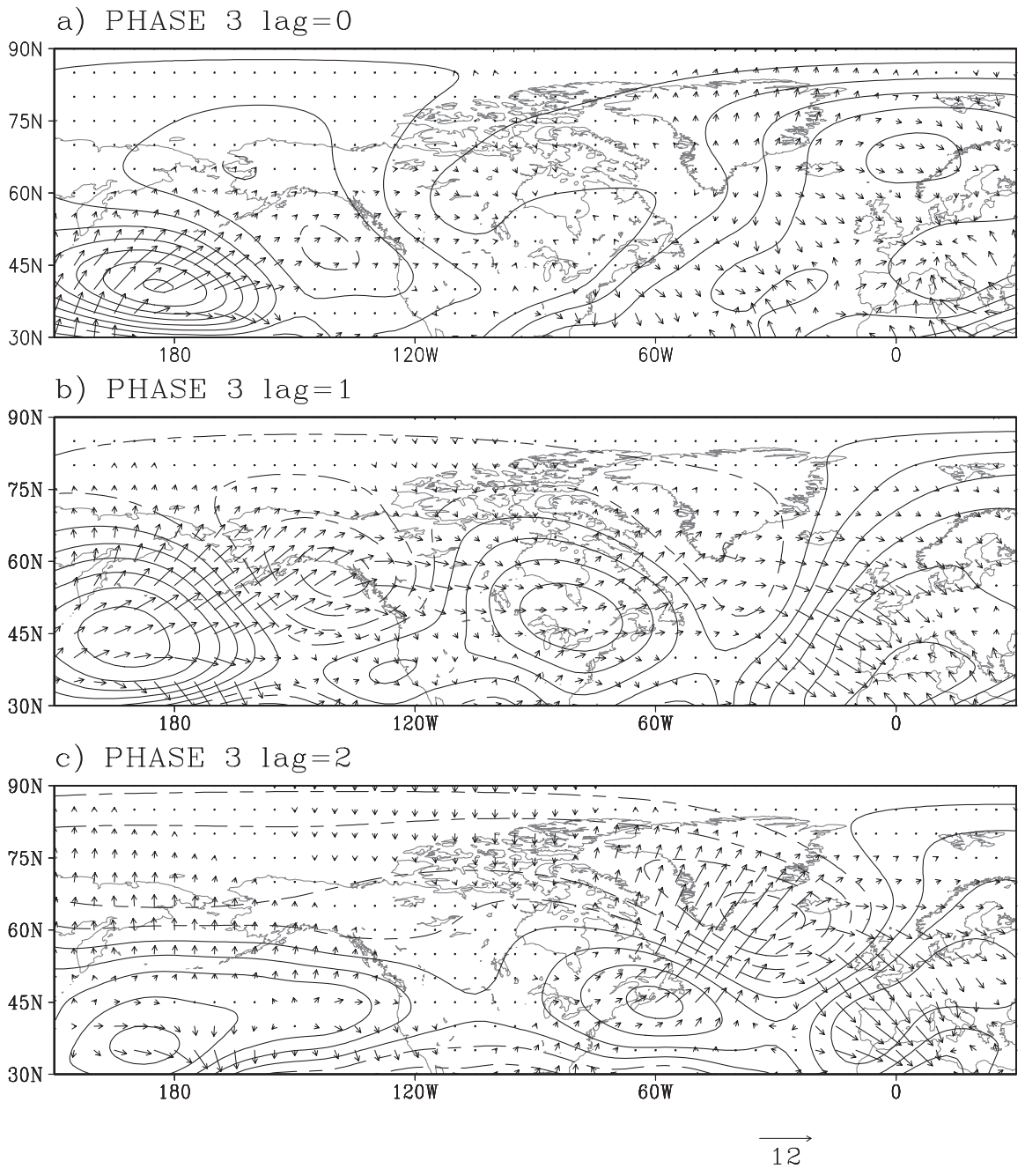

FIG. 5. 200-hPa wave activity flux with respect to MJO phase 3 for (a) lag 0, (b) lag 1, and (c) lag 2 pentads. The arrows are the horizontal (**W** vectors), and the contours the 200-hPa streamfunction anomalies. Contour interval is 1×10^6 m^2 s^{-1}. Contours with negative values are dashed. Scaling for arrows is given below (c) (unit: m^2 s^{-2}). Wave activity flux with magnitude smaller than 0.5 m^2 s^{-2} is not plotted.

shows that the tropical atmospheric response to the extratropical forcing in the North Atlantic leads to an eastward-propagating forced Kelvin wave in the tropical easterly mean flow of the Eastern Hemisphere. In this section, from a different angle, we investigate the influence of the NAO on the tropical Atlantic zonal wind. It is possible that an eastward expansion of the zonal wind anomaly in the tropical Atlantic contributes to trigger a development of the tropical intraseasonal variability in the Indian Ocean.

a. Climatology

The wintertime climatology in the Atlantic and African region is first analyzed. Shown in Fig. 6a is the 200-hPa

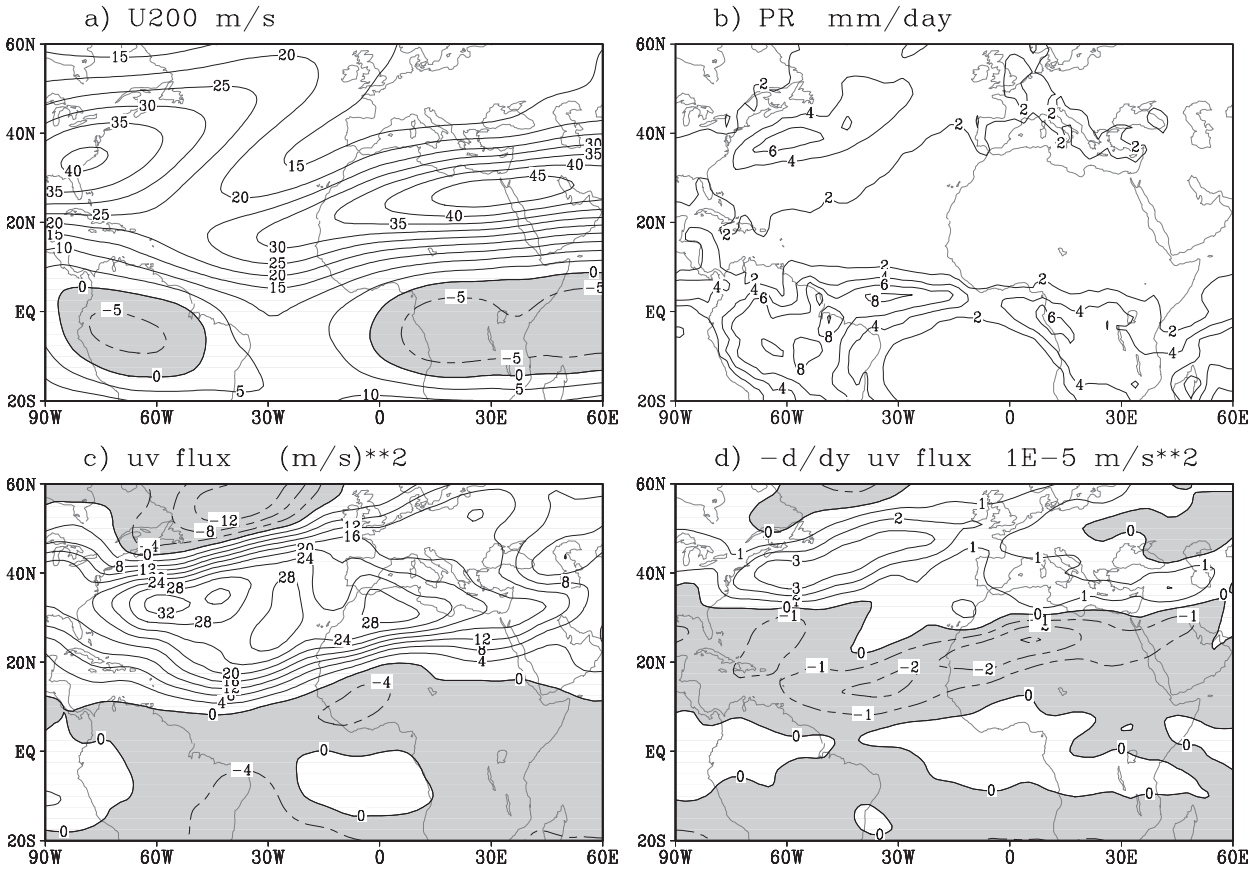

FIG. 6. Wintertime climatology in the Atlantic and African region for (a) 200-hPa zonal wind, (b) precipitation rate, (c) 200-hPa momentum flux by transients $\overline{u'v'}$, and (d) meridional convergence of the momentum flux by transients $-\partial\overline{u'v'}/\partial y$. Shaded areas in (a), (c), and (d) represent those with a negative value. Contour interval is 5 m s^{-1} for (a), 2 mm day^{-1} for (b), 4 m^2 s^{-2} for (c), and 1×10^{-5} m s^{-2} for (d). Contours with negative values are dashed.

zonal wind averaged over 25 extended winters. Tropical upper easterlies are found with maxima over equatorial America and the African–Indian Ocean region. The extratropics are dominated by westerlies. Two westerly jets are observed in the Atlantic and African sectors: one off the east coast of North America near 35°N, corresponding to the North American jet stream and storm track, and the other across North Africa near 25°N. The wintertime climatological precipitation rate is presented in Fig. 6b. Large precipitation is observed along the equator across the Atlantic. In the extratropics, associated with the North American jet stream, there is a band of heavy precipitation across the North Atlantic. The westerly jet over North Africa, however, is accompanied with minimum precipitation. As is known, synoptic transients contribute to the maintenance of extratropical westerly jets by transporting momentum. To estimate this effect, the momentum flux by transients is calculated for each pentad as $\overline{u'v'}$, where the overbar represents the pentad average, and the prime is the departure of daily data from the pentad average. Illustrated in Fig. 6c is the time mean 200-hPa transient momentum flux. Northward momentum flux is seen along the two westerly jets and the area in between, whereas southward momentum flux occurs to the north of 45°N and south of 5°N. The meridional convergence of the momentum flux by transients at 200-hPa level $-\partial\overline{u'v'}/\partial y$ is shown in Fig. 6d. Convergence of transient momentum flux is seen along the North American jet stream, accelerating the jet. The African jet, however, is accompanied by divergence of momentum flux, indicating that the transients are damping the jet over North Africa.

The different dynamics of the two extratropical westerly jets have been documented in previous studies (e.g., Blackmon et al. 1977; Lau 1979). Off the east coast of North America, the North American jet reaches its jet exit region, where the transients contribute to maintain its mean kinetic energy while the eddy heat flux reduces its vertical shear. The African jet, however,

develops as a result of thermally direct mean meridional circulation with upward motion in the tropics and descending motion near the jet.

b. Tropical Atlantic 200-hPa zonal wind associated with the MJO

Before looking at the influence of the NAO on the tropical intraseasonal variability, it is useful to see the signature of the MJO in the 200-hPa zonal wind in the tropical Atlantic–Indian Ocean sector. Shown in Fig. 7 are the simultaneous composites of the NCEP 200-hPa zonal wind anomaly for different MJO phases. In phase 1 (phase 5), an easterly (westerly) wind anomaly appears over Central America and the western Atlantic north of the equator. This zonal wind anomaly expands eastward across the tropical Atlantic. By phase 2 (phase 6), the easterly (westerly) wind anomaly covers the whole tropical Atlantic and Africa. As discussed in Hendon and Salby (1994), the MJO has a predominant Kelvin wave feature in the Western Hemisphere. The phase speed of the eastward propagation is about 15 m s^{-1}, which is in agreement with the phase speed of the forced Kelvin wave simulated by the SGCM in LBD07.

c. Lagged regressions of 200-hPa zonal wind to the NAO index

We now look at the lagged regression maps of atmospheric flow with respect to the NAO index, and see if there is any connection between the tropical circulation anomaly and the NAO variability in the Atlantic–African sector. The statistical significance of the linear regression is assessed using the Student's t test. Considering that the autocorrelation of the pentad data is not negligible, the effective sample size is estimated using the method discussed in Bretherton et al. (1999):

$$N' = N\left(\frac{1 - r_1 r_2}{1 + r_1 r_2}\right), \tag{2}$$

where N' is the effective sample size, N is the original sample size, and r_1 and r_2 are the lag 1 autocorrelation coefficients of the two time series involved. Since the lag 1 autocorrelation coefficient for the NAO index is 0.59, we have $N' = 0.48N$ assuming that $r_1 = r_2$.

Presented in Fig. 8 are the lagged regression maps of 200-hPa zonal wind with respect to the NAO index. Lag n indicates that the 200-hPa u lags the NAO index by n pentads. The magnitude represents $u200$ anomaly corresponding to one standard deviation of the NAO index. Shaded areas represent those where the correlation is statistically significant at a 0.01 level. From the simultaneous regression map (Fig. 8a), a familiar feature of the zonal wind associated with the NAO is evident that has been documented in previous studies (e.g., Hurrell 1995). A positive NAO is characterized by a northward shift of the North American jet, with a westerly anomaly along about 55°N and an easterly anomaly along about 30°N. Over the Atlantic region, a third westerly wind anomaly that is weak but significant is seen around 10°N in the tropics. The three bands of zonal wind anomalies with alternating signs constitute a tripole pattern over the North Atlantic. The temporal evolution of the 200-hPa zonal wind after a positive NAO can be visualized in the lagged regression maps (Figs. 8b–d). As the two zonal wind anomalies in the north weaken, the westerly anomaly near 10°N amplifies with time. This tropical westerly anomaly reaches its maximum about two pentads after the positive NAO. Therefore, a clear signal of southward propagation of the zonal wind anomaly amplitude is evident over the Atlantic region.

Using near-surface oceanic and atmospheric datasets and satellite measurements, Foltz and McPhaden (2004) presented evidence of intraseasonal oscillations in the trade winds in the tropical Atlantic. It was found that the variability in surface pressure and wind speed is associated with the NAO.

d. Transient momentum flux

It is of interest to understand what physical processes are responsible for the change of tropical zonal wind following a strong NAO as observed in Fig. 8.

A positive NAO is associated with a northward shift of the North American jet and the North Atlantic storm track (Fig. 8a). The anomalous easterly flow in the subtropical Atlantic near 30°N provides an environment that is unfavorable for an equatorward penetration of extratropical transient eddies (e.g., Webster and Holton 1982). This in turn will change the structure of the transient momentum flux and the dynamical feedback of transients to the mean flow. Shown in Fig. 9 are the lagged regression maps of 200-hPa transient momentum flux $\overline{u'v'}$ with respect to the NAO index. A positive NAO is accompanied by an increased northward momentum flux along the storm track (Fig. 9a). To the south, negative momentum flux anomalies are found in the subtropical Atlantic near 15°N, reflecting reduced transient activity due to less southward penetration of the extratropical transient eddies. The magnitude of the negative momentum flux anomaly increases with time and becomes a statistically significant feature in the subtropical Atlantic (Figs. 9b,c). This leads to an anomalous convergence of momentum flux near 10°N,

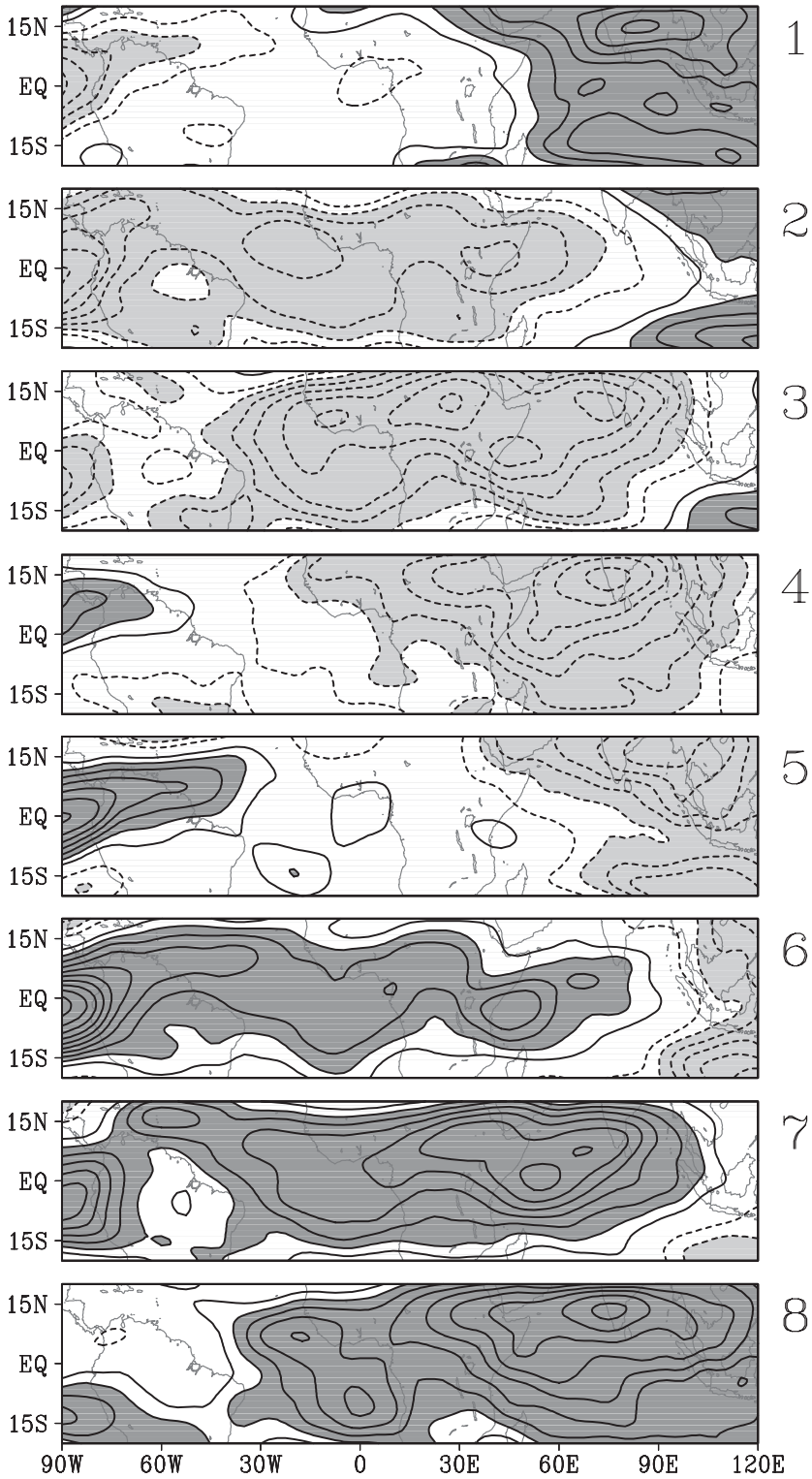

FIG. 7. Simultaneous composites of 200-hPa zonal wind anomaly in the tropical Atlantic–Indian Ocean sector for different MJO phases. The contour interval is 1 m s^{-1}. Contours of positive values are solid, while those for negative values are dashed. Zero line is not plotted. Shaded in dark gray are areas with wind anomaly greater than 2 m s^{-1}, whereas in light gray are those smaller than -2 m s^{-1}. The phase numbers are marked on the right of each panel.

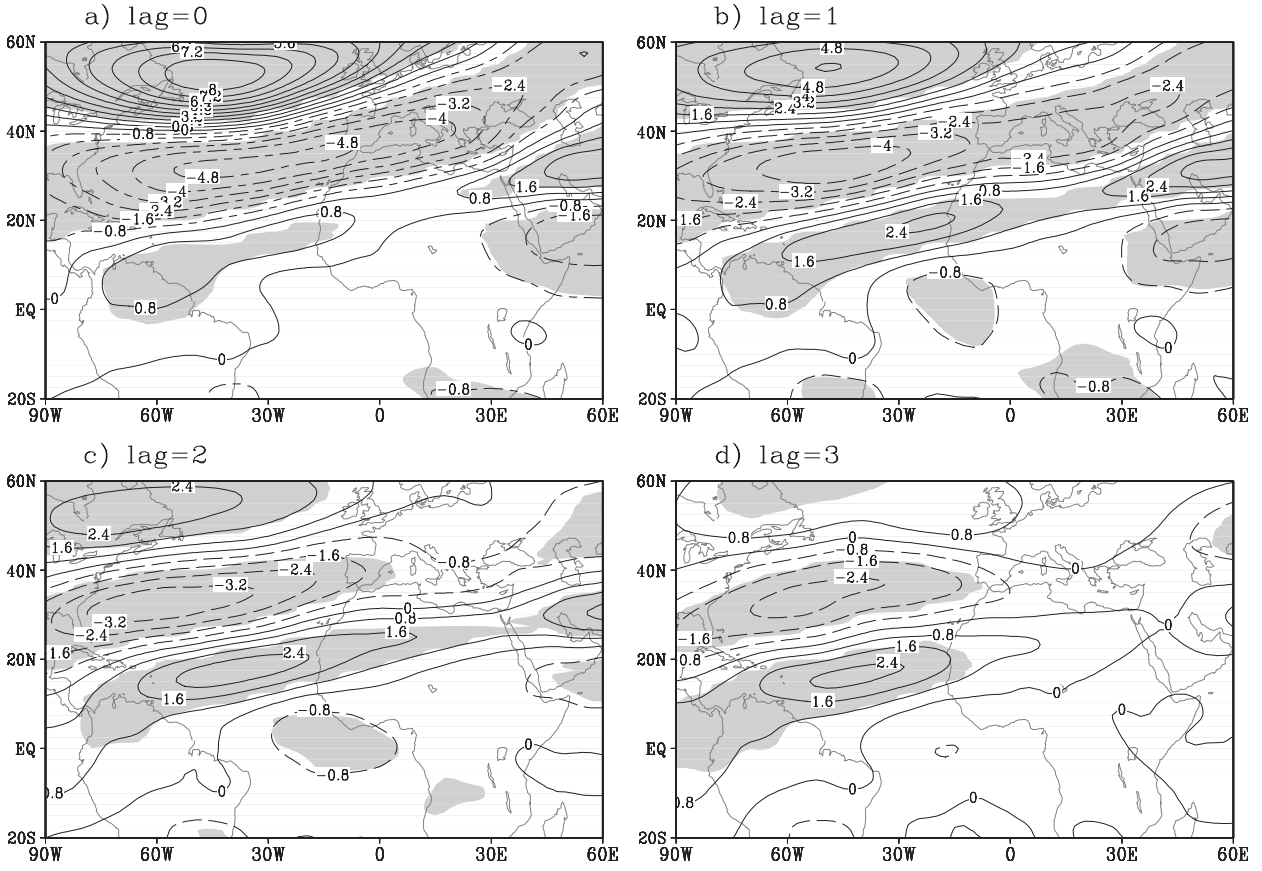

FIG. 8. Lagged regression maps of 200-hPa zonal wind with respect to the NAO index. Lag *n* indicates that the 200-hPa *n* lags the NAO index by *n* pentads. The magnitude represents *u* anomaly corresponding to one std dev of the NAO index. Contour interval is 0.8 m s^{-1}. Contours with negative values are dashed. Shaded areas represent those where the correlation is statistically significant at a 0.01 level.

which is confirmed by meridional convergence of the momentum flux $-\partial\overline{u'v'}/\partial y$ (not shown). It thus can be concluded that the increase of westerly wind near 10°N 2–3 pentads after a positive NAO (Fig. 8) is a direct result of the transient momentum flux convergence.

e. Consequence of tropical upper zonal wind changes

The acceleration and deceleration of the 200-hPa zonal wind in the tropical Atlantic by the transient momentum flux is connected to the tropical intraseasonal variability. Shown in Fig. 10 are the lagged regression maps of 200-hPa zonal wind in the tropical Atlantic between 20°S and 20°N with respect to the NAO index. Lag *n* indicates that the 200-hPa *u* lags the NAO index by *n* pentads. The first four panels in Fig. 10 are the same as Fig. 8 except for different regions. Shaded areas represent those where the regression is greater than 0.4 m s^{-1}. As can be seen, about 4 pentads after a positive NAO, a clear eastward expansion of the tropical westerly anomaly occurs. By lag 5 (the lowest panel), the zonal wind distribution becomes similar to that of phase 6 or phase 7 of the MJO (Fig. 7), though more concentrated north of the equator. Therefore, an acceleration of the 200-hPa westerly wind in the tropical Atlantic by the NAO may contribute to trigger and/or amplify phases 6 and 7 of the MJO. Indeed, as can be seen from Tables 2 and 3, a positive NAO is likely to lead phases 6 and 7 of the MJO by 2~5 pentads. Conversely, phases 2 and 3 of the MJO tend to follow a negative NAO.

The observed connection of the tropical intraseasonal variability to the NAO in this study is consistent with the model results as reported in LBD07. In that study, a long integration of a dry atmospheric model was conducted with time-independent forcing. The model was able to simulate a tropical intraseasonal variability that has many features similar to the MJO. Tropical–extratropical interactions were found to be responsible for significant intraseasonal variability in the model. An experiment with an anomalous vorticity forcing that represents the influence of the NAO showed that, in response to this forcing in the tropical Atlantic, a Kelvin wave that propagates eastward was generated.

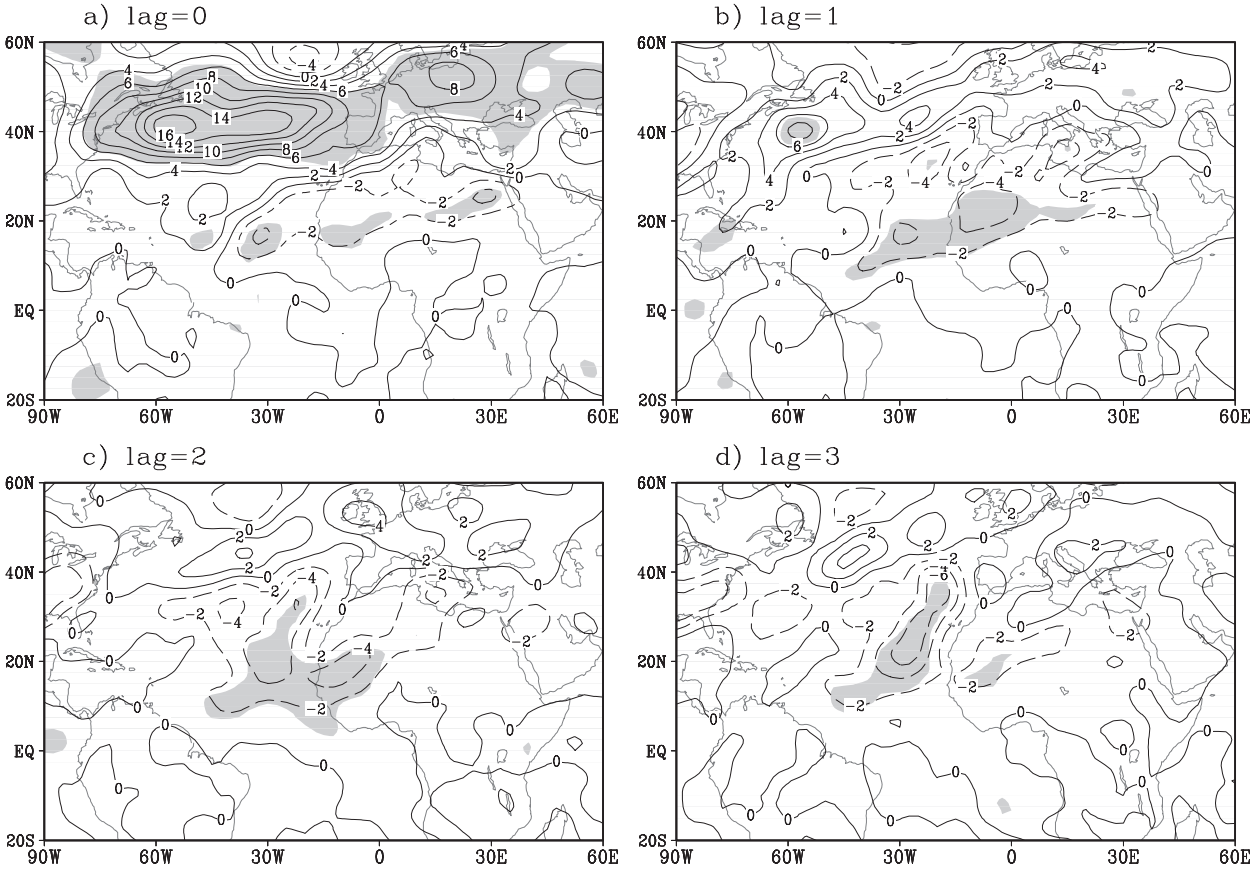

FIG. 9. Lagged regression maps of 200-hPa transient momentum flux with respect to the NAO index. The magnitude represents the anomaly corresponding to one std dev of the NAO index. Contour interval is 2 $m^2 s^{-2}$. Contours with negative values are dashed. Shaded areas represent those where the correlation is statistically significant at a 0.05 level.

A similar influence of the NAO on the tropical weather but on an interannual time scale has been reported in several previous studies. For example, Meehl and van Loon (1979) demonstrated that the seesaw in winter temperature between Greenland and northern Europe that is associated with the NAO is significantly correlated with the strength of the trade winds in the tropical Atlantic and with the precipitation over Africa. McHugh and Rogers (2001) found that the NAO index is negatively correlated with the precipitation in tropical eastern Africa in austral summer (December–February).

6. Summary and discussion

In this study we have examined the connection between the NAO the MJO, and the tropical–extratropical interaction on an intraseasonal time scale. Based on 25 yr (1979–2004) of pentad data and the bivariate MJO index in the boreal winter seasons, significant connections between the NAO and the tropical convection of the MJO are found. A prominent impact of the MJO on the North Atlantic localized NAO occurs after the MJO is observed in phases of 2–4 and 6–8; that is, a significant amplification of a positive (negative) NAO happens about 5–15 days after a depressed (enhanced) convection of the MJO reaches the tropical central Pacific region. An analysis of the evolution of the 500-hPa geopotential height anomaly indicates that the NAO is linked to the equatorial middle Pacific convection anomaly of the MJO through a Rossby wave train. The Rossby wave dispersion from the tropical Pacific to extratropical North Atlantic is supported by a wave activity flux analysis. On the other hand, in the North Atlantic sector, there is a significant influence of the NAO on the tropical intraseasonal variability. Lagged regression on the 200-hPa zonal wind with respect to the NAO index reveals a clear southward signal of amplitude of zonal wind anomaly in the North Atlantic, leading to a significant change of zonal wind across the tropical Atlantic. Further analysis indicates that this tropical zonal wind change is caused by a modulation of the momentum flux by high-frequency transients associated

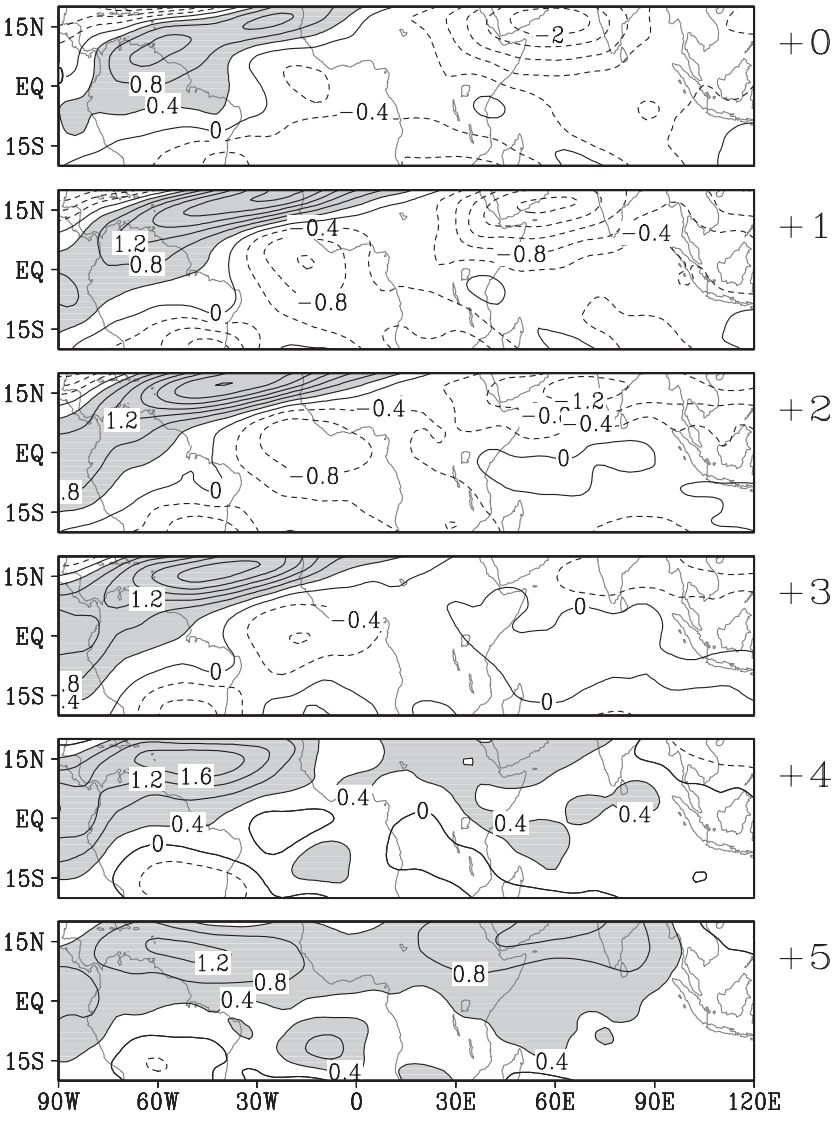

FIG. 10. Lagged regression maps of 200-hPa zonal wind in the tropical Atlantic with respect to the NAO index. Lag n indicates that the 200-hPa n lags the NAO index by n pentads. The magnitude represents u anomaly corresponding to one std dev of the NAO index. Contour interval is 0.4 m s^{-1}. Contours with negative values are dashed. Shaded areas represent those where the regression is greater than 0.4 m s^{-1}.

with the NAO variability. The 200-hPa zonal wind anomaly expands eastward in a similar way as a Kelvin wave. Along with enhanced tropical convection and precipitation, this may lead to an MJO development as the anomalous zonal wind and convection move into the warm water of the Indian Ocean.

Several studies have suggested a possible wintertime connection between the MJO and the extratropical AO (e.g., Zhou and Miller 2005; L'Heureux and Higgins 2008). It was demonstrated that when the MJO-related convection is enhanced (depressed) over the Indian Ocean, the AO tends to favor its positive (negative) polarity. In these studies, the phase of the AO was determined largely by its North Pacific center, which seems to have a more direct link with the tropical convection anomaly of the MJO. In the present study, the NAO is considered to be a local phenomenon in the North Atlantic sector that has a small simultaneous correlation with the North Pacific center of the AO. A significant remote impact on the NAO is found following the equatorial central Pacific convection anomaly of the MJO with a time lag of about 10 days. In other words, even without the contribution of the North Pacific sector as for the AO, there exists a significant

connection between the local NAO and the tropical convection of the MJO. This indicates that besides the extratropical internal dynamics, the tropical diabatic heating anomaly of the MJO provides another driving mechanism for the NAO variability. It is beyond the scope of this study to discuss the differences between the NAO and the AO. In fact they are likely indistinguishable (e.g., Feldstein and Franzke 2006), especially when the NAO is defined through an EOF analysis, as opposed to a two-point index (Jia et al. 2007). Our result indicates that a remote forcing of the MJO has a direct influence on the Atlantic sector of the NAO/AO.

With the observed lagged association of the NAO and the MJO, the possibility exists that a medium- and extended-range forecast of the NAO and its associated weather will benefit from a good knowledge of the MJO phase. Similarly, knowledge of the NAO would help to predict the MJO. Therefore, it is important for an operational numerical model to be able to simulate such an MJO–NAO connection.

An intriguing result of the present study is that a significant influence of the NAO on the tropical intraseasonal variability is observed in the Atlantic–African sector. A southward propagation of zonal wind signal in the upper-troposphere North Atlantic leads to a significant change of zonal wind in the tropical Atlantic. Further studies are needed to understand whether this modified zonal wind in the tropical Atlantic–Africa region triggers an MJO development, and if this is so, how the triggering proceeds. As discussed in LBD07, the southward wave activity flux in the subtropical Atlantic can excite a forced Kelvin wave in the tropical Atlantic and African sectors in a dry atmosphere. It is thus likely that the convective activity induced by upper zonal wind anomaly will interact with the intraseasonal variability of the dry dynamics and reinforce the MJO. Further studies are needed to better understand this process.

Acknowledgments. We thank Dr. Matthew Wheeler of the Centre for Australian Weather and Climate Research at the Bureau of Meteorology for making the MJO index available, and Dr. Xiaojing Jia of McGill University for useful discussions. We thank three anonymous reviewers whose comments and suggestions helped to improve our paper.

REFERENCES

Ambaum, M. H. P., B. J. Hoskins, and D. B. Stephenson, 2001: Arctic Oscillation or North Atlantic Oscillation? *J. Climate,* **14,** 3495–3507.

Baldwin, M. P., D. B. Stephenson, D. W. J. Thompson, T. J. Dunkerton, A. J. Charlton, and A. O'Neill, 2003: Stratospheric memory and extended-range weather forecasts. *Science,* **301,** 636–640.

Barnston, A. G., and R. E. Livezey, 1987: Classification, seasonality, and persistence of low-frequency atmospheric circulation patterns. *Mon. Wea. Rev.,* **115,** 1083–1126.

Blackmon, M. L., J. M. Wallace, N.-C. Lau, and S. L. Mullen, 1977: An observational study of the Northern Hemisphere wintertime circulation. *J. Atmos. Sci.,* **34,** 1040–1053.

Bretherton, C. S., M. Widmann, V. P. Dymnikov, J. M. Wallace, and I. Blad, 1999: The effective number of spatial degrees of freedom of a time-varying field. *J. Climate,* **12,** 1990–2009.

Cohen, J., K. Saito, and D. Entekhabi, 2001: The role of the Siberian high in Northern Hemisphere climate variability. *Geophys. Res. Lett.,* **28,** 299–302.

Deser, C., 2000: On the teleconnectivity of the Arctic Oscillation. *Geophys. Res. Lett.,* **27,** 779–782.

Emanuel, K. A., 1987: An air-sea interaction model of intraseasonal oscillations in the tropics. *J. Atmos. Sci.,* **44,** 2324–2340.

Feldstein, S. B., and C. Franzke, 2006: Are the North Atlantic Oscillation and the Northern Annular Mode distinguishable? *J. Atmos. Sci.,* **63,** 2915–2930.

Ferranti, L., T. N. Palmer, F. Molteni, and E. Klinker, 1990: Tropical-extratropical interaction associated with the 30–60 day oscillation and its impact on medium and extended range prediction. *J. Atmos. Sci.,* **47,** 2177–2199.

Foltz, G. R., and M. J. McPhaden, 2004: The 30–70 day oscillation in the tropical Atlantic. *Geophys. Res. Lett.,* **31,** L15205, doi:10.1029/2004GL020023.

Franzke, C., S. Lee, and S. B. Feldstein, 2004: Is the North Atlantic Oscillation a breaking wave? *J. Atmos. Sci.,* **61,** 145–160.

Greatbatch, R. J., H. Lin, J. Lu, K. A. Peterson, and J. Derome, 2003: Tropical/extratropical forcing of the AO/NAO: A corrigendum. *Geophys. Res. Lett.,* **30,** 1738, doi:10.1029/2003GL017406.

Hendon, H. H., and M. L. Salby, 1994: The life cycle of the Madden–Julian oscillation. *J. Atmos. Sci.,* **51,** 2225–2237.

Higgins, R. W., and K. C. Mo, 1997: Persistent North Pacific circulation anomalies and the tropical intraseasonal oscillation. *J. Climate,* **10,** 224–244.

Hoerling, M., A. Kumar, and M. Zhong, 1997: El Niño, La Niña, and the nonlinearity of their teleconnections. *J. Climate,* **10,** 1769–1786.

——, J. W. Hurrell, and T. Xu, 2001: Tropical origins for recent North Atlantic climate change. *Science,* **292,** 90–92.

Hsu, H.-H., 1996: Global view of the intraseasonal oscillation during Northern winter. *J. Climate,* **9,** 2386–2406.

——, B. J. Hoskins, and F. Jin, 1990: The 1985/86 intraseasonal oscillation and the role of the extratropics. *J. Atmos. Sci.,* **47,** 823–839.

Hu, Q., and D. R. Randall, 1994: Low-frequency oscillations in radiative–convective systems. *J. Atmos. Sci.,* **51,** 1089–1099.

Hurrell, J. W., 1995: Decadal trends in the North Atlantic Oscillation: Regional temperature and precipitation. *Science,* **269,** 676–679.

Jia, X., J. Derome, and H. Lin, 2007: Comparison of the life cycles of the NAO using different definitions. *J. Climate,* **20,** 5992–6011.

Jin, F., and B. J. Hoskins, 1995: The direct response to tropical heating in a baroclinic atmosphere. *J. Atmos. Sci.,* **52,** 307–319.

Johansson, Å., 2007: Prediction skill of the NAO and PNA from daily to seasonal time scales. *J. Climate,* **20,** 1957–1975.

Kalnay, E., and Coauthors, 1996: The NCEP/NCAR 40-Year Reanalysis Project. *Bull. Amer. Meteor. Soc.,* **77,** 437–471.

Knutson, T. R., and K. M. Weickmann, 1987: The 30–60 day atmospheric oscillation: Composite life cycles of convection and circulation anomalies. *Mon. Wea. Rev.,* **115,** 1407–1436.

Lau, K.-M., and T. J. Phillips, 1986: Coherent fluctuations of extratropical geopotential height and tropical convection in intraseasonal time scales. *J. Atmos. Sci.,* **43,** 1164–1181.

——, and L. Peng, 1987: Origin of low-frequency (intraseasonal) oscillations in the tropical atmosphere. Part I: Basic theory. *J. Atmos. Sci.,* **44,** 950–972.

Lau, N.-C., 1979: The structure and energetics of transient disturbances in the Northern Hemisphere wintertime circulation. *J. Atmos. Sci.,* **36,** 982–995.

L'Heureux, M. L., and R. W. Higgins, 2008: Boreal winter links between the Madden–Julian oscillation and the Arctic Oscillation. *J. Climate,* **21,** 3040–3050.

Li, S., M. P. Hoerling, S. Peng, and K. M. Weickmann, 2006: The annular response to tropical Pacific SST forcing. *J. Climate,* **19,** 1802–1819.

Liebmann, B., and D. L. Hartmann, 1984: An observational study of tropical-midlatitude interaction on intraseasonal time scales during winter. *J. Atmos. Sci.,* **41,** 3333–3350.

——, and C. A. Smith, 1996: Description of a complete (interpolated) outgoing longwave radiation dataset. *Bull. Amer. Meteor. Soc.,* **77,** 1275–1277.

Limpasuvan, V., and D. L. Hartmann, 1999: Eddies and the annular modes of climate variability. *Geophys. Res. Lett.,* **26,** 3133–3136.

Lin, H., J. Derome, and G. Brunet, 2005: Tropical Pacific link to the two dominant patterns of atmospheric variability. *Geophys. Res. Lett.,* **32,** L03801, doi:10.1029/2004GL021495.

——, G. Brunet, and J. Derome, 2007a: Intraseasonal variability in a dry atmospheric model. *J. Atmos. Sci.,* **64,** 2422–2441.

——, ——, and ——, 2007b: The nonlinear transient atmospheric response to tropical forcing. *J. Climate,* **20,** 5642–5665.

Madden, R. A., and P. R. Julian, 1971: Description of a 40–50 day oscillation in the zonal wind in the tropical Pacific. *J. Atmos. Sci.,* **28,** 702–708.

——, and ——, 1994: Observations of the 40–50 day tropical oscillation—A review. *Mon. Wea. Rev.,* **122,** 814–837.

Matthews, A. J., B. J. Hoskins, and M. Masutani, 2004: The global response to tropical heating in the Madden–Julian oscillation during Northern winter. *Quart. J. Roy. Meteor. Soc.,* **130,** 1991–2011.

McHugh, M. J., and J. C. Rogers, 2001: North Atlantic Oscillation influence on precipitation variability around the southeast African convergence zone. *J. Climate,* **14,** 3631–3642.

Meehl, G. A., and H. van Loon, 1979: The seesaw in winter temperatures between Greenland and Northern Europe. Part II: Teleconnections with lower latitudes. *Mon. Wea. Rev.,* **107,** 1095–1106.

Palmer, T. N., and Z.-B. Sun, 1985: A modelling and observational study of the relationship between sea surface temperature in the northwest Atlantic and the atmospheric general circulation. *Quart. J. Roy. Meteor. Soc.,* **111,** 947–975.

Peng, S., and J. S. Whitaker, 1999: Mechanisms determining the atmospheric response to midlatitude SST anomalies. *J. Climate,* **12,** 1393–1408.

Pozo-Vázquez, D., M. J. Esteban-Parra, F. S. Rodrigo, and Y. Castro-Díez, 2001: The association between ENSO and winter atmospheric circulation and temperature in the North Atlantic region. *J. Climate,* **14,** 3408–3420.

Sardeshmukh, P. D., and B. J. Hoskins, 1988: The generation of global rotational flow by steady idealized tropical divergence. *J. Atmos. Sci.,* **45,** 1228–1251.

Takaya, K., and H. Nakamura, 2001: A formulation of a phase-independent wave-activity flux for stationary and migratory quasigeostrophic eddies on a zonally varying basic flow. *J. Atmos. Sci.,* **58,** 608–627.

Thompson, D. W. J., and J. M. Wallace, 1998: The Arctic Oscillation signature in the wintertime geopotential height and temperature fields. *Geophys. Res. Lett.,* **25,** 1297–1300.

van Loon, H., and J. C. Rogers, 1978: The seesaw in winter temperatures between Greenland and Northern Europe. Part I: General description. *Mon. Wea. Rev.,* **106,** 296–310.

Wallace, J. M., and D. S. Gutzler, 1981: Teleconnections in the geopotential height field during the Northern Hemisphere winter. *Mon. Wea. Rev.,* **109,** 784–812.

——, and D. W. J. Thompson, 2002: The Pacific center of action of the Northern Hemisphere annular mode: Real or artifact? *J. Climate,* **15,** 1987–1991.

Wang, B., 1988: Dynamics of tropical low-frequency waves: An analysis of the moist Kelvin wave. *J. Atmos. Sci.,* **45,** 2051–2065.

Webster, P. J., and J. R. Holton, 1982: Cross-equatorial response to middle-latitude forcing in a zonally varying basic state. *J. Atmos. Sci.,* **39,** 722–733.

Wheeler, M., and H. H. Hendon, 2004: An all-season real-time multivariate MJO index: Development of an index for monitoring and prediction. *Mon. Wea. Rev.,* **132,** 1917–1932.

Xie, P., and P. A. Arkin, 1997: Global precipitation: A 17-year monthly analysis based on gauge observations, satellite estimates, and numerical model outputs. *Bull. Amer. Meteor. Soc.,* **78,** 2539–2558.

Zhang, C., 2005: Madden–Julian oscillation. *Rev. Geophys.,* **43,** RG2003, doi:10.1029/2004RG000158.

Zhou, S., and A. J. Miller, 2005: The interaction of the Madden–Julian oscillation and the Arctic oscillation. *J. Climate,* **18,** 143–159.